The s-wave in Mass A=7 + p Scattering

L. Buchmann for E1025

April 19, 2005

1   Introduction

The ^{7}Be+p scattering system has regained attention by the fact that a large fraction in the uncertainty of the ^{7}Be(p,γ)^{8}B S-factor at low energies comes from uncertainties in theoretical extrapolation. In particular, P. Descouvement [1] predicts that the ^{3}S$_{1(-)}$ wave in the elastic scattering has a positive phaseshift below 2 MeV from calculations by a cluster model, while potential models result in a negative phaseshift. The cluster model reproduces very well the energy dependence of the latest direct measurement of ^{7}Be(p,γ)^{8}B [2], while potential models do not. A measurement of the elastic ^{7}Be+p reaction has been reported in Ref. [3], however, the measurement is at too low energies and not of high enough precision to draw conclusions about the sign of the s-wave phaseshift.

The ^{7}Li+p reaction is an interesting case for testing experimental set-ups to do a high precision ^{7}Be+p experiment. It also allows develop analysis programs to obtain realistic phaseshifts as phaseshifts are not trivially derived from differential cross sections obtained in a measurement. We will discuss phaseshifts in the A=7+p system first. As we have obtained ^{7}Li+p elastic scattering data from a previous measurement, we will then discuss a phaseshift analysis of this measurement. At last we will see what difference in differential cross section (the observable) the predictions of Ref. [1] do actually produce.

2   Phaseshifts in the s=1 and s=2 mixed system

^{7}Li and ^{7}Be have a ground state spin of J$^\pi$=3/2$^-$, while the proton has a spin of J$^\pi$=1/2$^+$. Thus the channel spin is s=1 or 2, with negative parity states connected to the s-wave. R. G. Seyler [4] has treated the ^{7}Li+p system and given a general description how to proceed with a phaseshift analysis.

If we restrict ourselves to s-, p-, and d-waves, we find 16 scattering states ($^{2s+1}\ell_J$):
for s=1: ^{3}S$_1$, ^{3}P$_0$, ^{3}P$_1$, ^{3}P$_2$, ^{3}D$_1$, ^{3}D$_2$, ^{3}D$_3$;
for s=2: ^{5}S$_2$, ^{5}P$_1$, ^{5}P$_2$, ^{5}P$_3$, ^{5}D$_0$, ^{5}D$_1$, ^{5}D$_2$, ^{5}D$_3$, ^{5}D$_4$
while the the parity of these states goes with $\pi = (-)^{\ell+1}$. States with identical

J$^\pi$ are mixed, i.e. between S and D states and within the P states, resulting in 9 mixing parameters. J$^\pi$ therefore runs from 0^+ to 4^- (see table 1). L. Brown et al. [6] present a parameterization of the collision matrix $\mathbf{W}$ in terms of the phases and mixing parameters ordered by possible resonances with a given J$^\pi$. For $\ell \leq 2$ some of the states can be populated by up to three combinations of s and ℓ what is referred to in L. Brown et al. as channel. Then the nuclear part of the collision matrix is

$$\mathcal{W}^{J^\pi}_{c(m)c(n)} = \sum_{p=1}^{3} u^{J^\pi}_{pm} u^{J^\pi}_{pn} e^{2i\delta^{J^\pi}_{c(p)}} \tag{1}$$

with the face shifts $\delta_{c(p)}$ that are in general complex; $c(p)$ are order parameters as listed in table 1.

The coefficients $u^{J^\pi}_{pc}$ are given in term of the mixing parameters ϵ^{J^π}, ζ^{J^π}, and η^{J^π} by

$$
\begin{aligned}
u_{11} &= \cos\eta\cos\zeta \\
u_{12} &= \sin\eta\cos\zeta \\
u_{13} &= \sin\zeta \\
u_{21} &= -\cos\epsilon\sin\eta - \sin\epsilon\sin\zeta\cos\eta \\
u_{22} &= \cos\epsilon\cos\eta - \sin\epsilon\sin\zeta\sin\eta \\
u_{23} &= \sin\epsilon\cos\zeta \\
u_{31} &= \sin\epsilon\sin\eta - \cos\epsilon\sin\zeta\cos\eta \\
u_{32} &= -\sin\epsilon\cos\eta - \cos\epsilon\sin\zeta\sin\eta \\
u_{33} &= \cos\epsilon\cos\zeta
\end{aligned}
\tag{2}
$$

Nota bene that the first index for the coefficients u_{pc} refers to the summation index in Eq. 1 and the second index to the order index c in Table 1. We therefore get the combination of spins, channel spins, angular momenta and mixing parameters shown in table 1, which can be used as free parameters to fit the desired angular distributions. ϵ is a measure of channel spin mixing without ℓ mixing, ζ is a measure of ℓ mixing without s mixing, and η a measure of mixing between partial waves of different ℓ and s.

In equation 1, when there are only two elastic channel for any J$^\pi$ (table 1), the $p=1$ index in the sum should be dropped and $\eta=\zeta=0$, $c=2,3$; for the one channel case $U = e^{2i\delta^{J^\pi}_{s\ell}}$, i.e. for the stretched states in table 1. Then is, e.g. $(c(m)=1,c(n)=1)$ for the 1^- and the 2^- states

$$\mathcal{W}_{10,10} = u_{11}u_{11}\exp 2i\delta_{10} + u_{21}u_{21}\exp 2i\delta_{22} + u_{31}u_{31}\exp 2i\delta_{12} \tag{3}$$

and $(c(m)=1,c(n)=2)$

$$\mathcal{W}_{10,22} = u_{11}u_{12}\exp 2i\delta_{10} + u_{21}u_{22}\exp 2i\delta_{22} + u_{31}u_{32}\exp 2i\delta_{12} \tag{4}$$

J^π	$c=(s\ell)$	Parameters $\delta_{s\ell}^{J^\pi}$
0^-	(22)	$\delta_{22}^{0^-}$
0^+	(11)	$\delta_{11}^{0^+}$
1^-	1 (10)	$\delta_{10}^{1^-}$ $\delta_{22}^{1^-}$ $\delta_{12}^{1^-}$ ϵ^{1^-} ζ^{1^-} η^{1^-}
	2 (22)	”
	3 (12)	”
1^+	2 (11)	$\delta_{11}^{1^+}$ $\delta_{21}^{1^+}$ ϵ^{1^+}
	3 (21)	”
2^-	1 (20)	$\delta_{20}^{2^-}$ $\delta_{12}^{2^-}$ $\delta_{22}^{2^-}$ ϵ^{2^-} ζ^{2^-} η^{2^-}
	2 (12)	”
	3 (22)	”
2^+	2 (11)	$\delta_{11}^{2^+}$ $\delta_{21}^{2^+}$ ϵ^{2^+}
	3 (21)	”
3^-	2 (22)	$\delta_{22}^{3^-}$ $\delta_{12}^{3^-}$ ϵ^{3^-}
	3 (12)	”
3^+	(21)	$\delta_{21}^{3^+}$
4^-	(22)	$\delta_{22}^{4^-}$

Table 1: Combination of spins, channel spins, angular momenta and mixing parameters for $\ell \leq 2$ in ^{7}Be+p.(” same as above.)

etc..

The nuclear part of the collision matrix relates to the transition matrix $\mathbf{M}$ whose elements are given as follows:

$$
\begin{aligned}
M_{\alpha's'\nu',\alpha s\nu}(\theta_{\alpha'}) &= \frac{\sqrt{\pi}}{k_\alpha}[-C_{\alpha'}(\theta_{\alpha'})\delta_{ss',\nu\nu'} \\
&+i\sum_{j\ell\ell'}(2\ell+1)^{1/2}(s\ell\nu0|j\nu)(s'\ell'\nu'\nu-\nu'|j\nu) \\
&e^{i(\omega_\ell+\omega_{\ell'})}(\delta_{ss',ll'}-\mathcal{W}^j_{s'\ell's\ell})Y^{\nu-\nu'}_{\ell'}(\theta_{\alpha'},0)]
\end{aligned} \tag{5}
$$

with (|) being Clepsch-Gordan coefficients and $Y^{\nu-\nu'}_{\ell'}(\theta_{\alpha'},0)$ the spherical harmonics. ν and ν' represent possible magnetic substates of the channel spins s. Note that since $Y_{00}=\frac{1}{\sqrt{4\pi}}$ s-wave partial waves do not have a distinct angular distribution, but rather decrease or increase the cross section uniformly. $\mathcal{W}^j_{s'\ell's\ell}$ represents the nuclear part of the collision matrix. $C_{\alpha'}(\theta_{\alpha'})$ is the Coulomb amplitude.

Parity conservation forces

$$
M_{-\nu's',-\nu s} = (-)^{s'-s+\nu'-\nu}M_{\nu's',\nu s} \tag{6}
$$

reducing the number of elements of the matrix $\mathbf{M}$ to half.

The transition matrix relates then in the usual manner to the differential cross section:

$$
d\sigma_{\alpha s,\alpha's'} = (2s+1)^{-1}\sum_{\nu\nu'}|M_{\alpha s\nu,\alpha's'\nu'}(\Omega_{\alpha'})|^2 d\Omega_{\alpha'} \tag{7}
$$

All together, as the phaseshifts are complex, we have 41 real parameters to describe elastic scattering of the ^{7}A+p system, when s, p, and d waves are included. The imaginary parts of the phaseshift describe inelastic processes, but do not separate individual channels. However, as we will restrict the use of partial waves involved for practical reasons, individual inelastic channels will be associated with one particular partial wave.

3   Fits to the Warters data

3.1   Discussion of the data

In 1953 W.D. Waters et al. [5] published ^{7}Li+p elastic scattering data containing absolute cross sections, the only absolute cross sections for this reaction ever published to our knowledge. The data range from 359 keV to 1395 keV in the laboratory system and from 50° to 160°, i.e. stay below the (p,n) threshold. There are higher energy data available, normalized to Warters et al., but at this stage we have not included them in the fit.

In the Phys. Rev. publication of Warters et al. a note added in proof stated that these data have to be renormalized due to new stopping power measurements by 5% down. A private communication to the authors of Ref. [6] stated in addition that another lowering of the data by 4% was necessary. Both corrections are the result of improved stopping powers at the time. Using the quoted stopping power for the first correction, by today's best tables another 5% lowering would be adequate. However, we find that the 9% correction of Ref. [6] produces the most reasonable results, and we will quote those here. Ref. [5] do not give errors to their data, but claim an all over error of 5%. As we assume that statistics is of minor importance we assign this error to all data points, though somewhat larger errors may have been more adequate. Note that in Ref. [3] the ^{7}Be+p data are described as being normalized to those of Ref. [5], without mentioning what normalization has been used.

W.D. Warters gives excitation functions for seven angles, not always taken at the same energies. As the phaseshifts and mixing angles depend on energy, but not on angle, we have made interpolations to keep obtain angular distributions for a given energy, similar to Ref. [6]. Fig. 1 shows such an angular distribution.
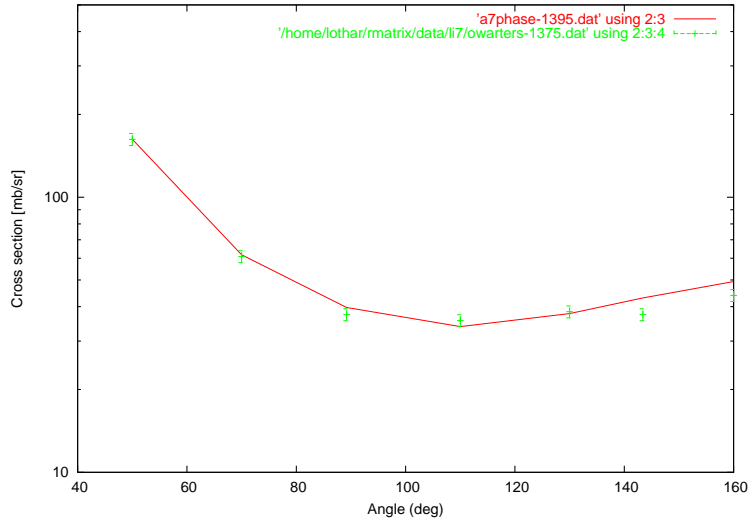

Figure 1: Angular distribution from Ref. [5](1395 keV) and fit to the data.

5

3.2 Individual fits

Using the formalism described in Section 2 fits to the individual angular distributions can be obtained. However, per energy point there are only 7 angles to be fitted by many more parameters. Even if free parameters are used sparingly, this results in very good fits to individual distributions, but very inconsistent phaseshifts, i.e. phaseshifts can fluctuate between close by energy points more than reasonable physics expectations would allow. Fig. 2 shows phaseshifts derived under the conditions discussed below.
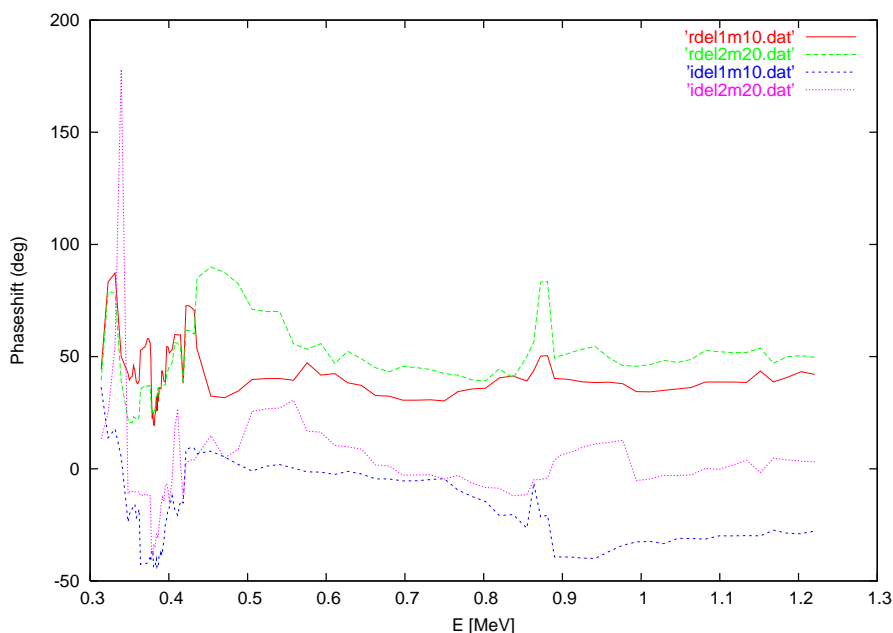

Figure 2: Real and imaginary parts of the 1^- and 2^- s waves in a free fit with 40 parameters. The $^5P_1$ wave has been fixed according to literature values for the 1^+ resonances.

Keeping neighbouring energy points uncorrelated, even the 1^+ resonance structure in the excitation function does not show up clearly, but manifests itself as strong p-wave fluctuations in the resonance energy region. Therefore, as a first step, the real part of the $^5P_1$ (abbreviated here 1p21 [1^+, s=2, ℓ=1]) wave was parametrized in terms of elastic scattering expressions from the R-matrix as

$$\delta_{1p21} = -\phi_{1p21} + \omega_{1p21} + \arctan \frac{R_{1p21}P_{1p21}}{1 - R_{1p21}(S_{1p21} + B_{1p21})} \ . \tag{8}$$

6

with ϕ being the hardsphere phaseshift, ω the Coulomb phaseshift and

$$R = \frac{\gamma^2}{E - E_r} \qquad (9)$$

the R-function, while S, P, and B are shift functions, penetrability, and boundary conditions in the usual R-matrix ways. This procedure ignores the multichannel character of the problem, i.e. mixed terms between inelastic and elastic channels. However, in this energy region such cross terms are likely irrelevant. In principle, more complex expressions can be implemented at a later stage. The boundary condition was set at E_b=386 keV, i.e. on the first narrow resonance, resonance energies and widths have been approximately matched to literature.

The s-wave phaseshifts shown in Fig. 2 have in the local fit the $^5P_1$ wave fixed in this global way, yet they still show strong fluctuations in the narrow resonance region at 386 keV and some correlation to the p-wave at about 0.95 MeV where a broad resonance is observed.

3.3   Global fits

It is obvious from multiple fit exercises that the individual phaseshifts need to be described by a few global parameters allowing for fits over the entire energy range of the data. While the structure of the 1^+21 phaseshift, showing obvious resonances, can be reasonably described by R matrix theory, this is not so clear with the other phaseshifts. In principle, a full R-matrix multichannel description will likely succeed in getting reasonable fits to the data. However, it would not be clear what the thus derived phaseshifts, which would be a mixture of hard sphere phaseshifts and far distant background and/or real states, would accomplish or if a model dependence would be introduced. As we wish to derive the phaseshifts rather straightforwardly from the data to compare to model predictions, we have chosen to describe them by polynomials of up to third order, except for the aforementioned p-wave where both the elastic and the inelastic part corresponding the (p,p') scattering into the first excited state of ^{7}Li at 478 keV is modeled according to simple R-matrix expressions. As we do not wish to employ all partial waves, in particular those of high angular momentum or high spin, we only use the following partial waves (we find the dependence from mixing parameters extremely week):

- 1^+21 ($^5P_1$): The resonant p-wave, two known resonances are in the energy range and a background state is also used. The inelastic (p,p') scattering, as observed for the upper state is included as a p wave decay in the imaginary part.

- 1^-10 ($^3S_1$): The real part of the phaseshift is described by a third order polynomial without a zero order term so that for zero energy the phaseshift is zero. The imaginary part, corresponding to (p,p') is described by a

second order polynomial multiplied by the s-wave p' penetrability so that there is no cross section below threshold.

- 2^-20 ($^5S_2$): The real part is as for the 1^-10 ($^3S_1$) case. No imaginary part has been included.

- 1^+11 ($^3P_1$): The real part is described by a second order polynomial.

- 2^-22 ($^5D_2$): The real part is described by a third order polynomial with no zero order. This term is the only d-wave included.

- 0^+11 ($^3P_0$): The imaginary part is described by a second order polynomial. It corresponds to the (p,α) reaction that for symmetry reasons can only proceed via 0^+, 2^+, 4^+ etc. T=0 states in ^8Be. No real part has been included.

- 3^+21 ($^5P_3$): The real part is represented by a second order polynomial. It has been included as there is a very strong 3^+ resonance just above the neutron threshold.

After optimization the partial waves as displayed in Figs. 3, 4, 5 were found. Fig. 4 also contains the least squares χ^2 for individual angular distributions. The real parts of the s-waves show a rather flat, but relatively high positive value. This is largely enforced by the behaviour in the region between the two 1^+ resonances. The imaginary part may be influenced by the upper 1^+ resonance which would be unphysical. The real part of the 1p21 wave have been described by resonances as discussed above. These two 1^+ states are well known in literature. Letting the R-matrix parameters float reproduced well the literature values. The imaginary part, corresponding to (p,p') also follows resonance behaviour. Again, the inelastic (p,p') transition is well known for the upper resonance, but is also known to have a non resonant part which we included in the s-wave. For the d-wave only the 2m22 wave has been used in the fit and is displayed in Fig. 5. There may be some (anti-)correlation with the 1^- wave. the relative high value for low energies may also compensate for experimental effects.

Fig. 4 also shows the least squares distribution for individual energy points. Regions of bad fit are around the narrow low energy resonance (actually a few points in the centre of the resonance have been taken out), and in the region from approximately 0.5 to 0.8 MeV, i.e. between the two 1^+ resonances. The high energy region, in contrast, shows reasonable fits.

The first case of the narrow resonance is most likely experimental. As the target has a finite thickness it will integrate over a rapidly changing angular distribution. Our calculations do not include such an integration as experimental information is sparse and an integration would take considerable computing time. As this case of a bad fir is understood, the necessary effort to include target thickness integration is not justified.
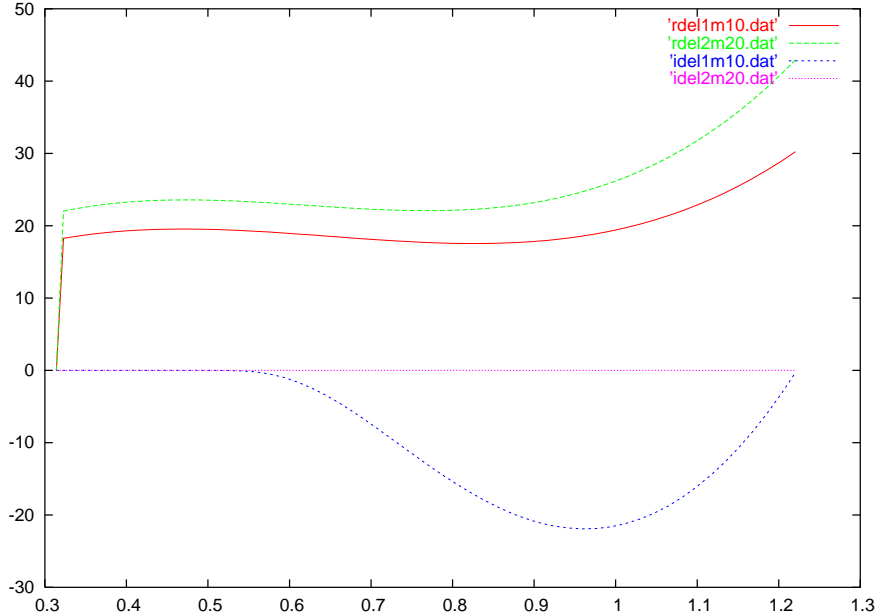
Figure 3: Real parts of the 1^- (red) and 2^- (green) s waves in degree in a global fit as described in the text versus cm energy. The imaginary part of the 1^- $s$wave is indicated in blue, while no imaginary part has been included for the 2^- wave. The lowest energy point has been set to a phase of zero.

The case of the inter-resonant region is less understood. In fact, Ref. [6] do not fit this region. We will see that this region would require a more sophisticated s-wave for a better description, while other waves are of no help. Inspecting angular distributions as derived shows that the deviations from a good fit are indeed systematic and not at random.

3.4 The least squares dependence of the 1m10 s-wave

We test now, how much a variation of one (1m10) of the two s-waves can be compensated for by the other waves, in particular the other (2m20) s-wave. It has been suggested in Ref. [6] that the 1m10 s wave should be of negative value. As for the best fit, as it is described by a polynomial with three coefficients, we apply a scaling factor to this polynomial to eventually reach negative phases. Thus we leave the shape of the 1m10 s-wave undistorted. The result is shown in Fig. 6. Obviously, the fit optimization with the rest of the global parameters being free finds no valid parameter to compensate for a change in the 1m10
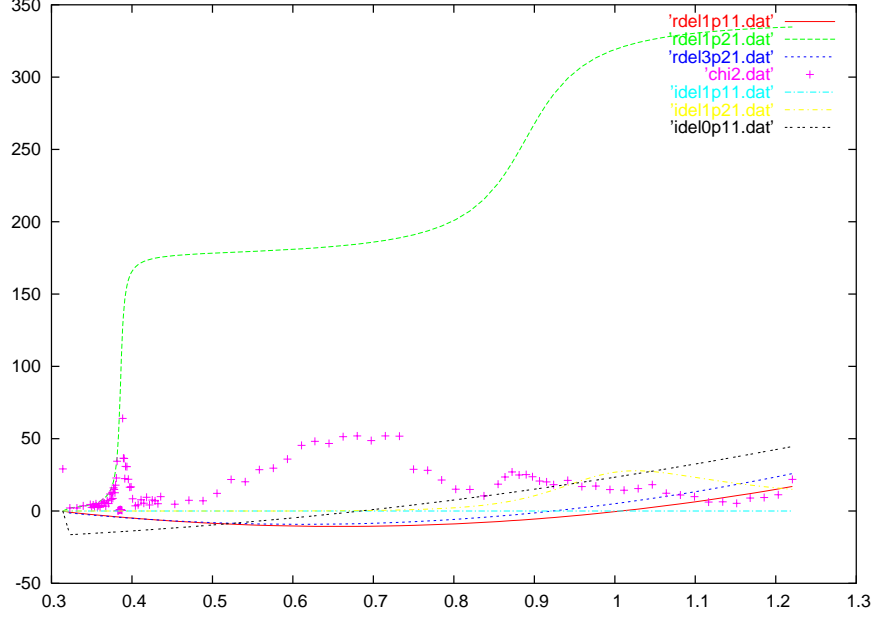
Figure 4: Real parts of the 1^+, s=1 (red) (1p11) and 1^* s=2 (green) (1p21) s waves in degrees in a global fit as described in the text versus cm energy. The imaginary part of the 1^+s=2 wave is indicated in yellow, also being resonant. All other waves included in the p-wave fit show gentle slope towards higher energies. The lowest energy point has been set to a phase of zero. Purple crosses indicate the individual χ^2 per energy point (no dimension).

wave. We present the result for the p-wave, including χ^2, and a scaling of -1 in Fig. 7. Obviously, the shape of the p-wave (and s-) wave remain largely unchanged. The least squares parameter χ^2 increases drastically in the 0.4 to 0.8 MeV region, while very high and very low energies remain reasonably fit. As an additional test, using the best parameters for the fit with the -1 scaling factor as a starting point, we let the 1m10 wave go free. Then the 1m10 wave went back into positive territory, albeit with a somewhat different (and worse) solution.

It is therefore concluded that the two s-waves are very well separable in the phaseshift fits to the data. However, the s-waves are particularly sensitive to the correct determination of the cross section.
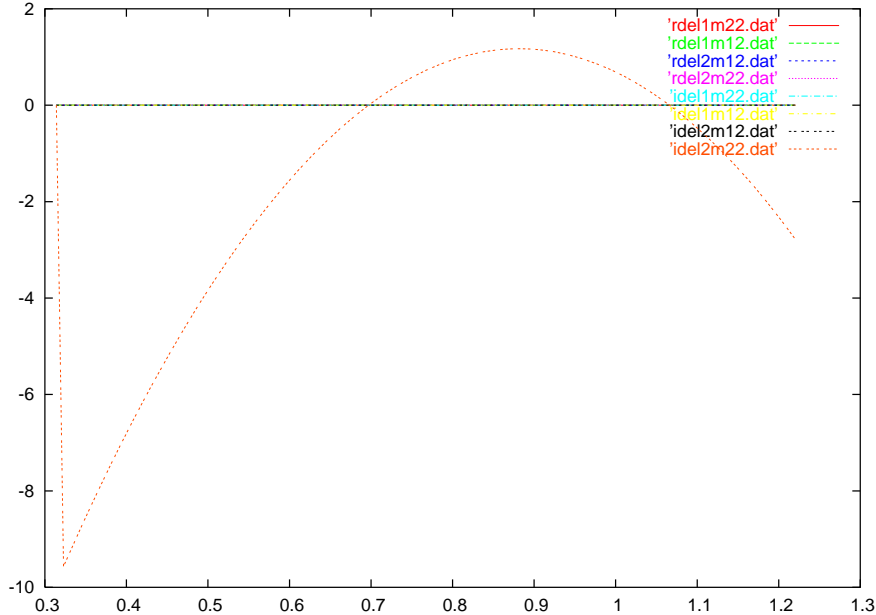
Figure 5: Real parts of the 2^- $s{=}2$, $\ell{=}2$ (2m22) (brown) d waves in degrees in a global fit as described in the text versus the cm energy. All other d-waves have been set to zero. The lowest energy point has been set to a phase of zero.

4 Predicted cross sections for ^{7}Be+p elastic scattering

From the predicted phaseshifts of Ref. [1] for the two s-waves cross sections can be deduced rather straightforwardly. However, the information of Ref. [1] is not complete as p-wave and d wave elastic contributions as well as all inelastic ones are not predicted. The known 1^+ and 3^+ resonances can be treated by an R-matrix approach as above, using literature values for energy and width. Since the inelastic (p,p') channel to the 418 keV first excited state in ^{7}Be is open, it has been included with an arbitrary width in both resonances. Other p and d waves or other inelastic channels are not included. For the s-waves a second order polynomial is chosen peaking at about $5°$ at 2 MeV. While this is not an exact match to the predicted phaseshifts of Ref. [1] it demonstrates the gross features of a sign change in the 1m10 wave. While the 1m10 wave changed sign the 2m20 wave was left constant.

Results are shown in Fig. 8. There is a clear difference in cross section

between the two cases. Numerically, the difference in cross section is 3.6% at 0.548 MeV, 12.6% at 1 MeV, 11.5% at 2 MeV and 4.6% at 3 MeV, normalized to the negative phaseshift case. For smaller angles, the differences naturally become smaller. Therefore, from these calculations, the region between 0.8 and 2 MeV looks rather promising to measure the difference in the sign of the phaseshift of the 1m10 wave.

5 Conclusions

The above fits and calculations demonstrate several points:

- To determine the phaseshifts of the s-wave, very good measurements of the absolute cross section of ^{7}Li/Be+p are necessary.

- Reasonable cross section data, i.e. 1-2% precision per point fix the individual s-wave (and other) phaseshifts in a unique way. The two s-wave phaseshifts cannot be traded against each other in fitting the data.

- The ^{7}Li+p data of Warters et al. [5] result probably in unphysical phaseshifts for some cases and should be remeasured. Note that these data have been used for normalization in many subsequent measurements.
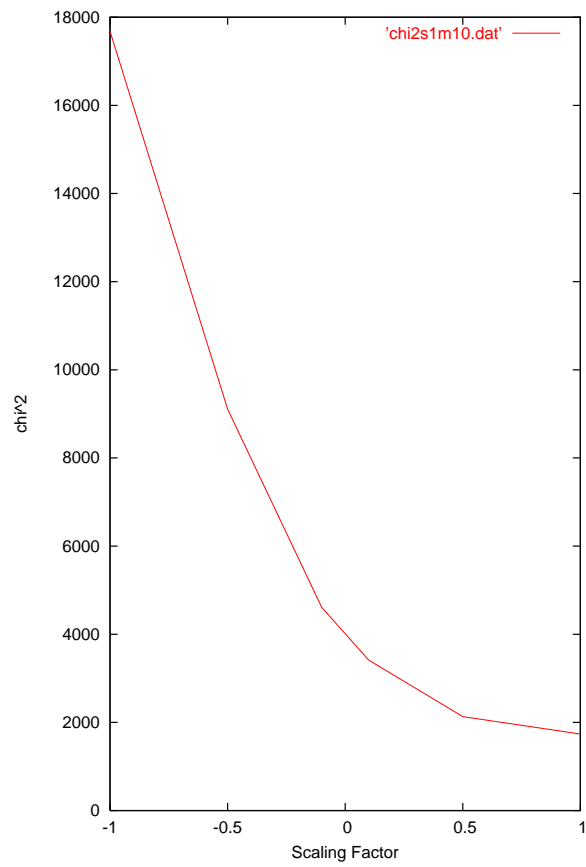
Figure 6: Least squares dependence of a scaling factor applied to the 1m10 wave. The scaling factor of 1 is the best fit.
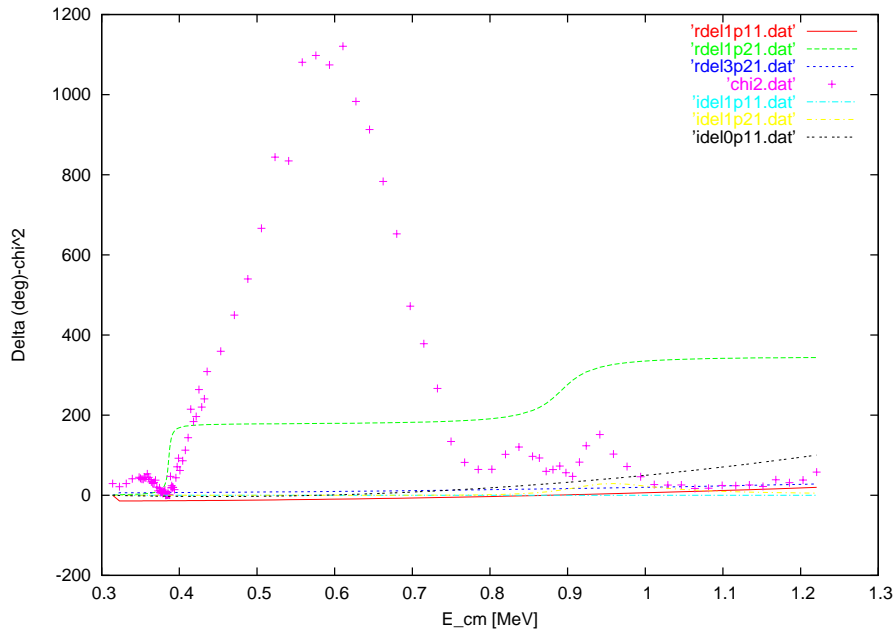
Figure 7: Real parts of the 1^+, $s=1$ (red) (1p11) and 1^* $s=2$ (green) (1p21) s waves in degrees in a global fit as described in the text versus cm energy for a scaling of the 1m10 s-wave of -1. The imaginary part of the $1^+ s=2$ wave is indicated in yellow, also being resonant. All other waves included in the p-wave fit show gentle slope towards higher energies. The lowest energy point has been set to a phase of zero. Purple crosses indicate the individual χ^2 per energy point (no dimension).
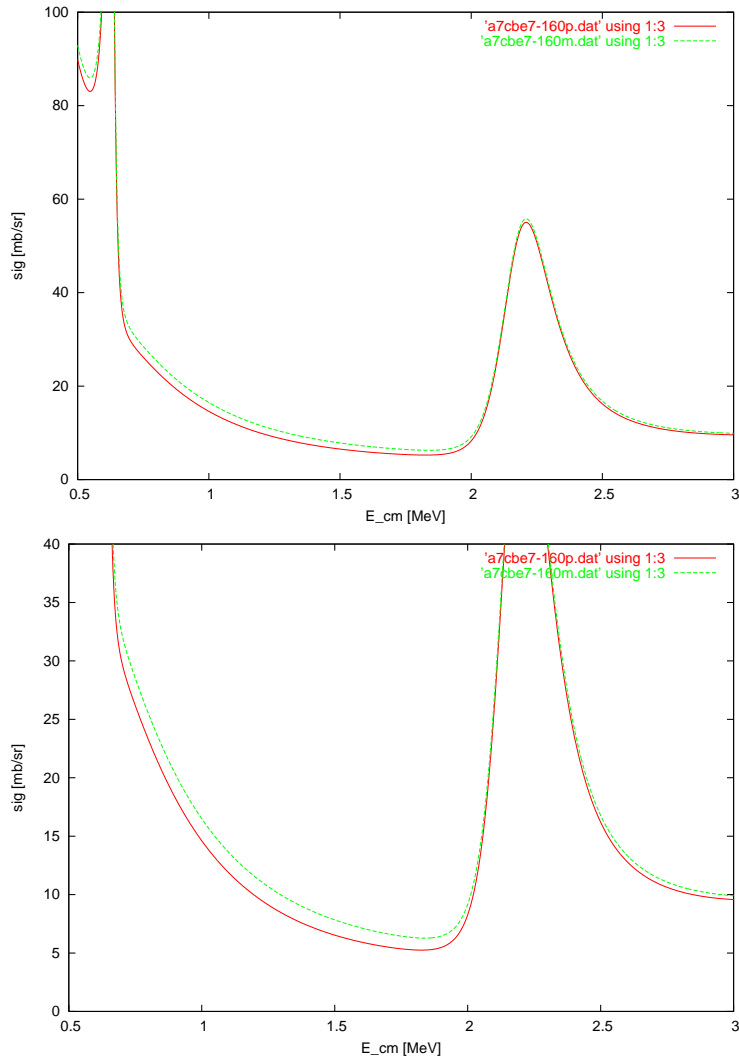
Figure 8: Calculated cross section for elastic scattering in ^{7}Be+p at 160°, cm. The upper and lower panels show two scales. The red line is for the 1m10 wave with a positive phase shift, the green line for a negative phase shift.

References

[1] P. Descouvement, Physical Review C, **70** (2004) 065802

[2] A. Junghans et al., Physical Review C, **68** (2003) 065803.

[3] C. Angulo et al., Nucl. Phys. A **716** (2003) 211.

[4] R.G. Seyler, Nucl. Phys. A **124** (1969) 253.

[5] W.D. Warters, W.A. Fowler, C.C. Lauritsen, Phys. Rev. **91** (1953) 917, and W.D. Warters, PhD thesis, Caltech 1953.

[6] L. Brown et al., Nucl. Phys. A **206** (1973) 353.